Oxygen reduction on a high-surface area Pt/Vulcan carbon catalyst: a thin-film rotating ring-disk electrode study

U.A. Paulus *, T.J. Schmidt [1], H.A. Gasteiger [2], R.J. Behm

Abteilung Oberflächenchemie und Katalyse, Universität Ulm, D-89069 Ulm, Germany

Abstract

We describe the adaptation of the recently developed thin-film rotating disk electrode method and its application in a rotating ring disk configuration (RRDE) to the investigation of the oxygen reduction reaction (orr) on a supported catalyst powder (Pt/Vulcan XC 72 carbon). This allows the determination of kinetic data, such as reaction orders or apparent activation energies, for the orr directly without mathematical modeling. Collection experiments reveal a potential and rotation rate independent collection efficiency. RRDE measurements allow, for the first time, the direct determination of the fraction of peroxide production during oxygen reduction on supported catalysts. Finally, comparison of measurements in 0.5 M H_2SO_4 and 0.5 M $HClO_4$, respectively, reveals a significant effect of (bi)sulfate adsorption on the orr activity. On the basis of the present results, predictions are made on the kinetic limit of the orr in polymer electrolyte fuel cells, in the absence of ohmic and mass transport resistances at 100% utilization. © 2001 Elsevier Science B.V. All rights reserved.

1. Introduction

Platinum supported on high surface area carbon substrates (e.g. Vulcan XC72) is still the most widely used electrocatalyst in low temperature polymer electrolyte fuel cells (PEM-FC) for both the anode and the cathode reaction [1]. While the overpotential for the anodic oxidation of pure hydrogen is negligible even at high current densities due to very facile H_2 oxidation kinetics on platinum, the strong kinetic inhibition of the cathodic oxygen reduction reaction (orr) leads to high overpotentials, amounting to several hundreds of millivolts under typical PEM-FC operating conditions [1]. Therefore, the slow orr kinetics on carbon supported Pt catalysts are the most limiting factor in the energy conversion efficiency of state-of-the-art PEM fuel cells

and the development of improved catalysts would have a dramatic impact on fuel cell efficiency. Due to the different electron yields of the two reaction paths (H_2O_2 versus H_2O formation), catalyst development for oxygen reduction catalysts requires that the electrocatalytic activity as well as the product distribution for the orr on new catalysts can be determined quantitatively under PEM-FC relevant conditions, i.e. continuous reactant flow, steady state, 60–80°C. We demonstrated this application recently for a Ru-chalcogenide catalyst [2].

Gloaguen et al. proposed the use of rotating disk electrode (RDE) measurements as a fast screening tool for the characterization of supported catalysts with respect to their orr activity [3]. They deposited a mixture of supported catalyst powder and Nafion® solution onto a glassy carbon disk and annealed this at 160°C to obtain a recast ionomer. As this preparation method results in a relatively thick catalyst layer (1–7 μm) with a high Nafion® content, film diffusion resistance plays an important role and extensive mathematical modeling is necessary to obtain the electrode kinetics from the measured RDE data [3,4]. Using the same experimental method, Gojkovic et al. [5] demonstrated a strong Nafion® film diffusion resistance using a Levich–

* Corresponding author. Present address: Paul Scherrer Institut, General Energy, CH-5232 Villigen PSI, Switzerland. Tel.: +41-56-3102059; fax: +41-56-3104415.

E-mail address: ursula.paulus@psi.ch (U.A. Paulus).

[1] Present address: Lawrence Berkeley National Laboratory, University of California, Berkeley, CA 94720, USA.

[2] Present address: GM Global R&D, Global Alt. Propulsion Center, 10 Carriage St., Honeoye Falls, NY 14472, USA.

Koutecky-type analysis of the orr currents, yielding Nafion® film diffusion limited current densities, j_f, of ca. 8 mA cm^{-2}. Since this is on the same order of magnitude as the overall current densities accessible with the RDE technique in aqueous electrolytes, Nafion® film diffusion resistances strongly hamper the extraction of kinetic current densities from these measurements.

We recently developed a method of thin-film RDE measurements [6], where small amounts of catalyst suspension are attached to a glassy carbon RDE by means of a sub-micrometer thick Nafion® film. As will be shown, this method results in ten-fold larger j_f values for the orr compared to the above method. This way, Nafion® film diffusion resistances become negligible within the accessible current density range at typical rotation rates up to 3600 rpm, and kinetic current densities can be extracted directly using the unmodified mass-transport correlations for a simple (i.e. smooth) RDE [7]. The significantly reduced catalyst loading used in the thin-film RDE method expands the range of experimentally accessible mass-specific current densities to values which are typically obtained in PEM fuel cells (i.e. 1–2 A mg$_{Pt}^{-1}$, corresponding to 1 A cm^{-2} at typical Pt-loadings of 1.0–0.5 mg$_{Pt}$ cm^{-2}). This allows the direct extrapolation of RDE data on the performance of PEM fuel cell electrodes.

The thin-film RDE technique can also be applied to rotating ring-disk electrodes (RRDE) which allows detailed study of the orr [2]. In this case, the extent of hydrogen peroxide formation during the orr (i.e. the so-called two-electron pathway) can be determined in parallel to the overall orr activity. RRDE measurements during the orr on supported Pt catalysts were previously reported by Claude et al. [8], but again the large loading of both Nafion® and catalyst restricted quantification of the H$_2$O$_2$ formation to very low rotation rates (ca. 100 rpm) since the collection efficiency was not stable at higher rotation rates. In contrast, the thin-film RRDE method allows much higher rotation rates, concomitant with an extended potential range where currents are controlled kinetically so that higher (and more relevant) mass-specific current densities become accessible.

The following study examines the O$_2$ reduction kinetics on a high-surface area Vulcan XC72 carbon supported platinum catalyst (referred to as Pt/Vulcan) using the thin-film RRDE technique. The data show that the film diffusion resistance of the Nafion® film is negligible for the orr. Simple ring-disk collection experiments with a Pt/Vulcan catalyst in a RRDE configuration demonstrate that a potential and rotation rate independent collection efficiency is achieved up to rotation rates of 2500 rpm. The well defined collection efficiency allows for an accurate determination of the fraction of H$_2$O$_2$ produced during the orr on Pt/Vulcan

at 60°C. To our knowledge this is the first exact determination of the O$_2$ reduction pathways on a supported Pt/Vulcan carbon catalyst, particularly at elevated temperatures. The obtained mass-specific current densities will be used to estimate the kinetic limits for PEM-FC performance using standard Pt/Vulcan carbon catalysts.

2. Experimental

For the measurements described in this study we used a commercially available catalyst of 20 wt.% platinum supported on Vulcan XC72 (E-TEK). Prior to electrochemical measurements, the catalyst was conditioned in a tube furnace in order to remove surface contaminants as described in Ref. [6]. The resulting particle size distribution and the dispersion, D, were determined by high resolution transmission electron microscopy ($d = 3.7 \pm 1$ nm, $D = 26\%$) [6].

The electrochemical measurements were conducted in a thermostated standard three-compartment electrochemical cell using an interchangeable ring-disk electrode setup with a bi-potentiostat and rotation control (Pine Instruments). The Pt ring electrode was potentiostated at 1.2 V (RHE) where the detection of peroxide is diffusion limited. Potentials were determined using a saturated calomel electrode (SCE), separated from the working electrode compartment by a closed electrolyte bridge in order to avoid chloride contamination. All potentials in this study, however, refer to that of the reversible hydrogen electrode (RHE).

Electrodes were prepared as described by Schmidt et al. [6]. In short, aqueous suspensions of 1 mg$_{catalyst}$ ml^{-1} were obtained by ultrasonic mixing for about 15 min. Glassy carbon disk electrodes (6 mm diameter, 0.283 cm^2, Sigradur G, Hochtemperaturwerkstoffe GmbH) served as the substrate for the supported catalyst and were polished to a mirror finish (0.05 μm alumina, Buehler). An aliquot of 20 μl catalyst suspension was pipetted onto the carbon substrate, leading to a Pt loading of 14 μg$_{pt}$ cm^{-2}. The Pt-loading was found to be reproducible within $\pm$ 6% based on a series of experiments in which cyclic voltammogramms were evaluated with respect to the hydrogen adsorption charge [9]. After evaporation of the water in an argon stream, 20 μl of a diluted Nafion® solution (5 wt.%, Fluka) were pipeted on the electrode surface in order to attach the catalyst particles onto the glassy carbon RDE, yielding a Nafion® film thickness of ca. 0.1 μm (the ratio of H$_2$O/Nafion® solution was ca. 100/1).

Comparing TEM dispersion and the H-adsorption charge indicates a utilization of the Pt/Vulcan catalyst of essentially 100% [6]. At the applied loading (14 μg$_{Pt}$ cm^{-2}) and the above determined Pt dispersion of 26%, the roughness factor of the electrode is ca. 9.1 (cm^2)$_{real}$/

$(cm^2)_{geometric}$, calculated under the commonly applied assumption that the atomic surface density of the Pt crystallites is roughly equal to the average atomic surface density of the low-index Pt single crystal planes (i.e. 1.23×10^{15} atoms $cm^{-2} \equiv 2.04 \times 10^{-9}$ mol cm^{-2}) [10,11]. Using this convention, the active Pt surface area for the 20 wt.% Pt/Vulcan carbon catalyst amounts to 65 m^2 g_{Pt}^{-1}.

After preparation, the electrodes were immersed in deaerated (Argon, Westfalen N6.0) 0.5 M H_2SO_4 or 0.5 M $HClO_4$ (Merck suprapure) under potential control at 0.1 V, if not specified otherwise. Owing to slight contamination from the Nafion® solution, the electrode potential was cycled several times between 0.05 and 1.4 V in order to produce a clean electrode surface. For the oxygen reduction experiments the electrolyte was saturated with oxygen (Westfalen N5.7) or with O_2 in Ar mixtures, produced using electronic mass flow controllers (MKS). Current densities are normalized either to the geometric area of the glassy carbon substrate (0.283 cm^2) or to the Pt-loading on the electrode.

With respect to the following oxygen reduction measurements it should be noted that the glassy carbon RDE and the pure Vulcan carbon at a loading of 56 μg_{Vulcan} cm^{-2} (equal to that used in the Pt catalyst experiments) did not show any appreciable oxygen reduction activity at potentials positive of 0.3 V, in agreement with Ref. [5]. Measurable oxygen reduction currents occurred only at potentials negative of 0.3 V, predominantly producing H_2O_2 (ca. 70%), as expected for a pure carbon electrode [12]. Nevertheless, the overall activity of the support material and the glassy carbon RDE were negligible in the entire potential range compared to the Pt/Vulcan catalyst.
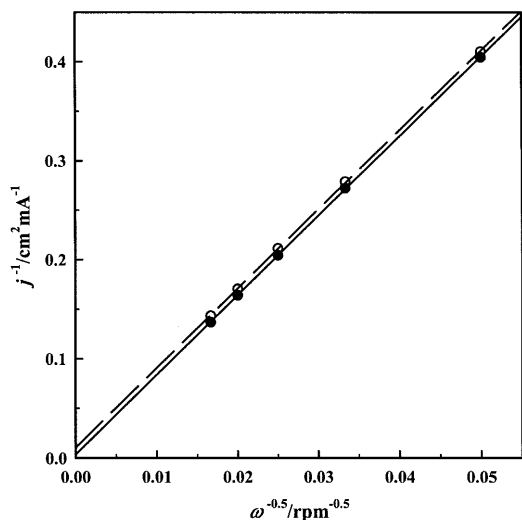

Fig. 1. Koutecky–Levich plots for O_2 reduction on a Pt/Vulcan (14 μg_{Pt} cm^{-2}) thin-film R(R)DE with a 0.1 μm Nafion® film (open circles, dashed linear regression line) and on a polycrystalline Pt-disk (solid circles, solid linear regression line). 60°C, 0.5 M H_2SO_4, 5 mV s^{-1}

3. Determination of experimental parameters for thin-film RRDE measurements

3.1. Nafion® film effects

Closely following the method described in Ref. [6], we varied the Nafion® film thickness from 15 to 0.1 μm (calculated from the covered electrode area of 0.283 cm^2 and assuming a film density of 2.0 g cm^{-3}) in order to determine the film diffusion resistance in the Nafion® film during O_2 reduction in 0.5 M H_2SO_4 at 60°C. Similarly to our results for the hydrogen oxidation reaction [6], the Nafion® film diffusion resistance becomes negligible for a film thickness smaller than 0.2 μm. Qualitatively, this is confirmed by the fact that the diffusion limited current densities obtained on Pt/Vulcan in the thin-film R(R)DE configuration (ca. 0.1 μm thick Nafion® film) are only ca. 5% smaller than those recorded on a smooth polycrystalline Pt-disk, even at rotation rates up to 3600 rpm. Much larger deviations ($\geq 25\%$) from the ideal RDE mass transport are found in RDE studies where high Nafion® and catalyst loadings were used [3–5,8].

To determine quantitatively the lower limit of the Nafion® film diffusion limited current density, j_f, the measured current density, j, is described by the following relation [13]:

$$\frac{1}{j} = \frac{1}{j_k} + \frac{1}{j_d} + \frac{1}{j_f} = \frac{1}{j_k} + \frac{1}{Bc_0\omega^{1/2}} + \frac{L}{nFc_fD_f} \quad (1)$$

where j_k and j_d are the kinetically and diffusion-limited current densities, respectively. The same relation was used previously for smooth Pt-RDE [14] and for Pt/Vulcan thin-film RDE experiments [7]. The other parameters are the Levich constant B, the reactant concentration in the solution c_0, the film thickness L, the reactant concentration in the Nafion® film c_f, and the diffusion constant in the Nafion® film D_f. On smooth electrodes, the j_f term in Eq. (1) does not exist and j depends only on j_k and j_d (see Eq. (2)). If the film thickness can be reduced to the extent that j_f becomes significantly larger than j_k and j_d, then the influence of j_f on the measured current density is negligible. This was tested for the present situation in the Levich–Koutecky plots obtained for a 14 μg cm^{-2} Pt/Vulcan electrode with a 0.1 μm thick Nafion® film (open circles) and for a polycrystalline Pt-disk (solid circles) at 60°C, which are shown in Fig. 1. Consistent with Eq. (1), the product Bc_0 obtained from the slope of the lines is nearly identical with the values obtained for the supported electrode and for the smooth Pt-disk, with 12.49×10^{-2} mA cm^{-2} $rpm^{-0.5}$ and 12.46×10^{-2} mA cm^{-2} $rpm^{-0.5}$ respectively. Based on Eq. (1), the intercept corresponds to the kinetic resistance ($1/j_k$) in the case of the smooth Pt-R(R)DE, and to the sum $1/j_k + 1/j_f$ in the case of the thin-film R(R)DE. Since the
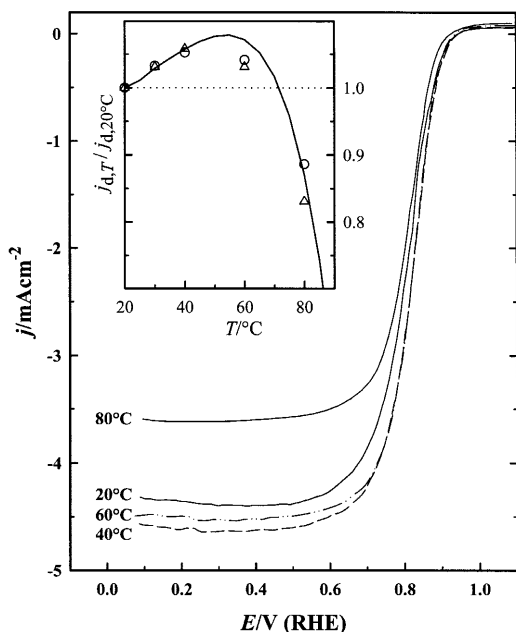
Fig. 2. Potentiodynamic (5 mV s^{-1}) oxygen reduction current densities on a thin-film Pt/Vulcan R(R)DE at 1600 rpm as a function of temperature (for clarity, the j/E curve for the 30°C data is not shown). Inset: theoretical temperature dependence of the diffusion limited current densities assuming the physical-chemical properties of pure water based on Eq. (7) (—) and experimental values obtained from two independent measurements (circles and triangles). 0.5 M H$_2$SO$_4$, 1 bar O$_2$, 14 μg$_{Pt}$ cm^{-2}.

inverse of the intercept of the smooth Pt-R(R)DE of 280 mA cm^{-2} is not much larger than the value of 94 mA cm^{-2} determined for the thin-film Pt/Vulcan R(R)DE, it can be concluded that the minimum Nafion® film diffusion limited current density is about equal to this value, 94 mA cm^{-2}. For the present low Pt loading (14 mg$_{Pt}$ cm^{-2}) this corresponds to a mass specific current density of ca. 6.7 A mg$_{Pt}^{-1}$, well within the mass-specific current density range in PEM-FC applications. The contribution of the film diffusion resistance to the measured current density should be negligible, if values of j_k determined from [15]:

$$\frac{1}{j} = \frac{1}{j_k} + \frac{1}{j_d} \tag{2}$$

are less than 25% of the value of j_f, i.e. less than ca. 24 mA cm^{-2} (corresponding to ≤ 1.5 A mg$_{Pt}^{-1}$). To conclude, PEM-FC relevant mass-specific current densities on the order of 1–2 A mg$_{Pt}^{-1}$ can be extracted from the current density in thin-film RDE measurements simply using Eq. (2), without encountering significant interference from Nafion® film diffusion resistances. This is not true in the case of the higher Nafion® and catalyst loadings applied in previous studies [3–5,8]. For example, much lower j_f values of ca. 8 mA cm^{-2}, corresponding to 0.2 A mg$_{Pt}^{-1}$ (Pt loading of ca. 40 μg$_{Pt}$ cm^{-2}) were observed by Gojkovic et al. [5]. Without

additional modeling of diffusion resistances produced by the Nafion® film and the catalyst agglomerate layer, this would lead to large errors in the evaluation of the true kinetic current density at mass-specific current densities above 0.05–0.1 A mg$_{Pt}^{-1}$, thereby limiting the utility of this approach to extract fuel cell relevant oxygen reduction kinetics.

3.2. RDE-specific temperature effects

In the following we will briefly discuss an artifact which can occur in R(R)DE experiments at high temperature. Fig. 2 presents the oxygen reduction currents on a Pt/Vulcan electrode at different temperatures between 20°C and 80°C at 1600 rpm in 0.5 M H$_2$SO$_4$ saturated with pure O$_2$ (1 bar).

Up to a temperature of 60°C, the diffusion limited current densities are nearly constant. At 80°C, a distinct decrease in current density is visible. In order to understand the temperature dependence of the diffusion limited current density, it is most logical to examine first the temperature dependence of the physical-chemical parameters in the Levich equation:

$$j_{d,RDE} = 0.620nFD^{2/3}v^{-1/6}c_0\omega^{1/2} \tag{3}$$

where D is the O$_2$ diffusion coefficient in the electrolyte, v is the kinematic viscosity, and ω is the rotation rate. The temperature dependence of the diffusion coefficient of a dissolved gas is described by the ratio of temperature, T (in K), and the dynamic viscosity, η [16]:

$$D \propto \frac{T}{\eta} \tag{4}$$

Eq. (4) can then be substituted in the Levich equation (Eq. (3)), in which the kinematic viscosity can also be re-expressed by the ratio of dynamic viscosity to electrolyte density, ρ:

$$v = \frac{\eta}{\rho} \tag{5}$$

Taking into consideration that c_0 is the concentration of dissolved oxygen at an oxygen partial pressure of 1 bar and that we are working in an open system with a total system pressure of ca. 1 bar (i.e. $p_{O_2} + p_{H_2O} = 1$ bar), the temperature dependence of the diffusion limited current densities based on Eqs. (3)–(5) is:

$$j_d \propto \frac{T^{2/3}\rho^{1/6}}{\eta^{5/6}}c_0(1 - p_{H_2O}) = P_T c_0(1 - p_{H_2O}) \tag{6}$$

The solid line in the inset in Fig. 2 shows the normalized (to j_d at 20°C) temperature dependence of the limiting current density for the orr as determined from Eq. (7) where c_T describes the concentration of dissolved oxygen at the temperature T and P_T is a constant which summarizes temperature, electrolyte density and kinematic viscosity. There it is assumed

that the temperature dependence of viscosity, O_2 solubility, and density for the dilute acid is the same as for pure water (data for pure H_2O from Ref. [17]):

$$\frac{j_{d,T}}{j_{d,20°C}} = \frac{P_T c_T (1 - p_{H_2O,T})}{P_{20°C} c_{20°C} (1 - p_{H_2O,20°C})} \qquad (7)$$

Based on this relation, the diffusion limited current densities are predicted to remain nearly constant in the temperature range between 20°C and 60°C, with a local maximum at about 55°C. At temperatures above 60°C, the predicted j_d values start to decrease rapidly owing to a drastic increase in the vapor pressure of water.

A comparison with the experimental data (Fig. 2, circles and triangles) demonstrates that the temperature dependence of j_d observed in O_2-saturated 0.5 M H_2SO_4 on a Pt/Vulcan thin-film R(R)DE is in reasonably good agreement with the above prediction. Therefore, the observed decrease of j_d for the orr at high temperatures is well described by the temperature dependence of the physical-chemical constants in the Levich equation (Eq. (3)) and does not result from temperature-induced changes in the Nafion® film
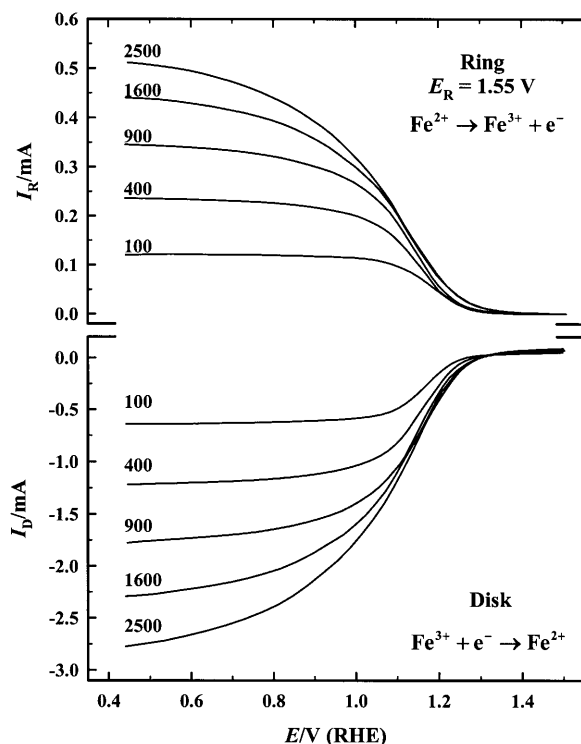
properties. As a consequence, the effective O_2 partial pressure in the framework of the above model decreases significantly at temperatures exceeding 60°C. For example, while the O_2 partial pressure is still ca. 0.8 bar at 60°C, p_{O_2} drops to ca. 0.5 bar at 80°C ($p_{H_2O} \approx 0.5$ bar), leading to a decrease of the feed gas partial pressure by a factor 2 with respect to the nominal pressure of 1 bar. For first order reactions, as is the case for the orr (see below), this would affect significantly the measured kinetics and has to be considered if data at different temperatures are being compared (e.g. in determining the activation energy). In particular, for the latter reason we have restricted all further orr measurements up to a temperature of 60°C.

3.3. Collection efficiency of the thin-film Pt/Vulcan RRDE

For the collection experiments, the electrodes were prepared as described above. The electrolyte was deaerated 0.1 M NaOH (Merck p.a.) with 10 mmol l^{-1} $K_3Fe(CN)_6$ (Merck p.a.), a typical compound for the determination of the collection efficiency [18]. The ring and the disk currents in the positive sweep direction (20 mV s^{-1}) at 60°C and at a constant ring potential of 1.55 V are shown in Fig. 3. At this ring potential, the oxidation of $[Fe(CN)_6]^{4-}$, which is produced at the disk electrode, to $[Fe(CN)_6]^{3-}$, proceeds under pure diffusion control, while oxygen evolution currents at the Pt-ring are still negligible. The collection efficiency is then determined from the ring (I_R) and disk (I_D) currents (in units of mA) [15]:

$$N = -\frac{I_R}{I_D} \qquad (8)$$

Within the examined potential range and at rotation rates up to 2500 rpm, the collection efficiency remains unchanged at $N = 0.19 \pm 0.01$, as evaluated from three independent experiments. The same value of N was also found when this experiment was carried out with a smooth polycrystalline Pt-disk in the same electrode holder.

From the similarity in the collection efficiencies obtained on smooth and supported electrodes it is clear that well defined RRDE measurements with supported electrocatalysts are possible using the thin-film RRDE method and that the intermediates (e.g. H_2O_2) detected at the ring electrode can be correctly quantified. In contrast to findings of Claude et al. [8], we obtained a constant, well defined collection efficiency even at high rotation rates (2500 rpm versus ≤ 100 rpm in Ref. [8]), where PEM-FC relevant mass-specific current densities are accessible.
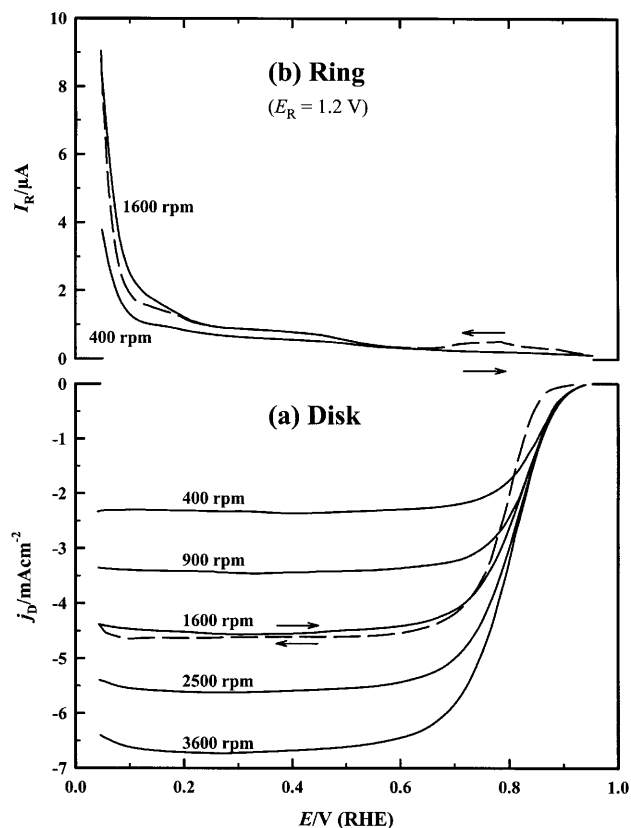

Fig. 3. Ring ($Fe^{2+} \rightarrow Fe^{3+} + e^-$) and disk ($Fe^{3+} + e^- \rightarrow Fe^{2+}$) currents at 60°C for the determination of the collection efficiency on a Pt/Vulcan (14 μg_{Pt} cm^{-2}) thin-film RRDE in 0.1 M NaOH supporting electrolyte with 10 mM $K_3Fe(CN)_6$. Positive sweeps at 20 mV s^{-1}; $E_{Ring} = 1.55$ V.

Fig. 4. (a) Potentiodynamic (5 mV s^{-1}, positive sweep) O_2 reduction current densities (j_D) on a thin-film RRDE with Pt/Vulcan catalyst (14 μg_{Pt} cm^{-2}) at 60°C in 0.5 M H_2SO_4 saturated with 1 bar O_2. (b) Simultaneously recorded ring currents (I_R) at 400 and 1600 rpm for a ring potential of $E_R = 1.2$ V. The dashed lines show the negative going sweeps at 1600 rpm.

4. Results and discussion

4.1. O_2 reduction activity of Pt/Vulcan catalyst at 60°C

Recent studies showed that the orr follows a complex reaction scheme, described, e.g., in Ref. [19]. The most important feature in that scheme, which we will concentrate on also in the following, is that the reduction of oxygen is known to proceed either in a four-electron step to H_2O or in a two-electron step to H_2O_2. In general, the four-electron step is considered the major reaction pathway on polycrystalline platinum electrodes in impurity-free aqueous acidic electrolytes [12,20,21]. The four-electron step is also the major reaction pathway on platinum single crystals, with the exception of Pt(111) and Pt(100) surfaces where at potentials within the hydrogen adsorption/desorption region (H_{upd} region, $E < 0.3$ V), oxygen is reduced nearly quantitatively to H_2O_2 [22–24]. Since carbon supported platinum catalysts typically consist of cubo-octahedral nanocrystallites with a large fraction of (100) and (111) facets for particle sizes above 2 nm [23,25], one might

expect that the orr on the Pt/Vulcan catalyst ($\bar{d}_{Pt} = 3.7$ nm) resembles the behavior of Pt(111) and Pt(100).

Fig. 4a shows the oxygen reduction current densities for the positive sweep on a Pt/Vulcan disk electrode (14 μg_{Pt}cm^{-2} in 0.5 M H_2SO_4 at 60°C). In agreement with the behavior observed on Pt single crystals [22–24], on polycrystalline Pt [26,27], and on carbon supported platinum [5], the orr is under mixed kinetic-diffusion control in the potential range between 0.9 and 0.6 V, followed by a region where diffusion limiting currents can be observed. Although it is shown only for one rotation rate (1600 rpm), the orr activity in the negative sweep direction (dashed line in Fig. 4a) is always lower than in the positive sweep direction (solid lines in Fig. 4a) for potentials positive of 0.7 V, equivalent to a potential shift of 20 to 30 mV. This effect was already observed previously on both polycrystalline and carbon supported platinum [5,27]. As an explanation Gottesfeld et al. [27] suggested that the strong hysteresis in Pt surface oxide formation/reduction in combination with the lower orr activity in the presence of Pt surface oxides is responsible for the lower orr activity in the negative sweeps. Close to the hydrogen evolution region, a slight decrease of the disk current densities can be observed in Fig. 4a, particularly at high rotation rates. Based on previous RRDE experiments with Pt single crystals [22–24] and polycrystalline Pt [26], this is related to the onset of H_2O_2 formation rather than a loss in orr activity (see Section 4.2).

4.2. Orr pathway on a Pt/Vulcan catalyst at 60°C

The reaction pathway of the orr, i.e. the relative formation rates of H_2O and H_2O_2, can be determined quantitatively with an RRDE experiment by setting the potential of the ring electrode at 1.2 V, where the oxidation of the H_2O_2 formed by O_2 reduction on the disk electrode is diffusion limited.

For the positive sweeps of the above described O_2 reduction experiment, Fig. 4b shows that ring currents are negligible in the potential region above 0.6 V, indicating that at potentials relevant to fuel cell cathodes, reduction of O_2 proceeds exclusively via a complete four-electron step. H_2O_2 formation becomes apparent only at potentials negative of 0.6 V and increases significantly in the H_{upd} region. Closer inspection shows that the appearance of ring currents follows quantitatively the decrease in disk currents from its diffusion limited value as expected for a change in the orr pathway from a four- to a two-electron pathway.

The slight increase in H_2O_2 formation at < 0.6 V and its strong enhancement within the H_{upd} region (~ 0.2 V) on the Pt/Vulcan catalyst is analogous to polycrystalline platinum (25°C, 0.05 M H_2SO_4) [26] and agrees quantitatively with the H_2O_2 formation reported for a Pt(110) electrode in 0.05 M H_2SO_4 at 25 and 60°C

[22,24]. The strong enhancement in the H_{upd} region is generally attributed to hydrogen (co-)adsorption, which blocks the dissociation of molecularly adsorbed hydrogen. On the other hand, the formation of H_2O_2 (Fig. 4b) is dramatically different from what was observed for Pt(111) and Pt(100) single crystals [24] which is particularly astonishing considering that the carbon supported small Pt particles used in this study should exhibit large fractions of Pt(111) and Pt(100) sites [12,23]. For the latter surfaces, RRDE experiments performed under comparable conditions (60°C, 0.05 M H_2SO_4) demonstrated a nearly 100% transition from a four- to a two-electron pathway in the hydrogen adsorption region, which the authors related to a 'special state of H_{upd}' [24]. Based on this discrepancy, one might expect that the platinum crystallites on the supported catalyst do not exhibit these large fractions of (111) and (100) facets predicted by thermodynamics. It will be shown below, however, that the orr activity on Pt/Vulcan in the kinetically controlled region ($E > 0.7$ V) is entirely consistent with the predominance of Pt(100) and Pt(111) facets. Therefore, this inconsistency in H_2O_2 formation is explained tentatively by a high H_2O_2 decomposition activity of low coordinated Pt atoms (edge and corner atoms), an issue which could be resolved by experiments on a stepped single crystal.

Similar to the effect of a hydrogen adlayer on Pt(111) and Pt(100) described above, it was shown that other strong adsorbates can also inhibit the complete four-electron reduction of O_2. For instance, enhanced H_2O_2 formation is observed in the presence of organic adsorbates [26], of bromide anions [28] or in the presence of surface oxides, e.g. for Pt(111) and Pt(100) in alkaline solutions [29]. The latter finding agrees well with the present observation of enhanced H_2O_2 formation during the negative sweep (see dashed line in Fig. 4b) in a potential range where Pt surface oxides are present.

Owing to the deleterious effect of H_2O_2 on the stability of polymer electrolyte membranes, the extent of H_2O_2 formation on the cathode catalyst in the potential region above ca. 0.7 V (i.e. at the typical operating potential) is a critical criterion for the choice of suitable catalysts. This is crucial, however, not only for the orr but also for the anode reaction. Oxygen reduction to H_2O_2 may also occur on the anode catalyst at the typical operating potential of below ca. 0.1 V, since molecular O_2 can come in contact with the anode catalyst either due to the significant O_2 cross-over through thin state-of-the-art membranes (e.g. Nafion® 112 and GORE Select) or via the air-bleed used for operation with reformat [1]. The data shown in Fig. 4 can be used to evaluate the fraction of H_2O_2 produced during the orr (Fig. 5).

Taking into account that the total disk current, I_D, is the sum of the O_2 reduction currents to water, I_{H_2O}, and to H_2O_2, $I_{H_2O_2}$ (Eq. (9)), and using the collection efficiency N as defined in Eq. (8)

$$I_D = I_{H_2O} + I_{H_2O_2} \text{ with } I_{H_2O_2} = I_R N^{-1} \tag{9}$$

the fraction of H_2O_2 formation, $X_{H_2O_2}$, can be calculated from the molar flux rates of O_2, $\dot{n}_{O_2(4e-)}$, and H_2O_2, $\dot{n}_{O_2(2e-)}$, according to Eqs. (10) and (11):

$$\dot{n}_{O_2(4e-)} = I_{H_2O}/4F \text{ and } \dot{n}_{O_2(2e-)} = I_{H_2O_2}/2F \tag{10}$$

$$X_{H_2O_2} = \frac{\dot{n}_{O_2(2e-)}}{\dot{n}_{O_2(2e-)} + \dot{n}_{O_2(4e-)}} = \frac{2I_R/N}{I_D + I_R/N} \tag{11}$$

The maximum peroxide production occurs at potentials negative of 0.1 V, reaching levels of 5–6%. Hence, under these conditions significant amounts of H_2O_2 are expected to be produced via oxygen crossover at the membrane│anode catalyst interface. At the typical cathode operating condition of 0.7–0.8 V, however, H_2O_2 formation at steady state (i.e. on an oxide-free platinum surface) is close to the quantification limit of ca. 0.2%. These values are independent of the rotation rate and essentially independent of temperature (data not shown), in accordance with the results obtained at Pt single crystals [24]. The fraction of H_2O_2 produced on Pt/Vulcan in the H_{upd} region at 0.1 V, of about 5–6% is much lower than that produced on either Pt(111) (ca. 70%) or Pt(100) (ca. 35%) [24].

4.3. Oxygen reduction reaction order with respect to oxygen partial pressure

For the evaluation of kinetic current densities from thin-film R(R)DE data on the Pt/Vulcan catalyst, Eq. (2) is only correct for a reaction order of one with respect to p_{O_2}. The reaction order with respect to
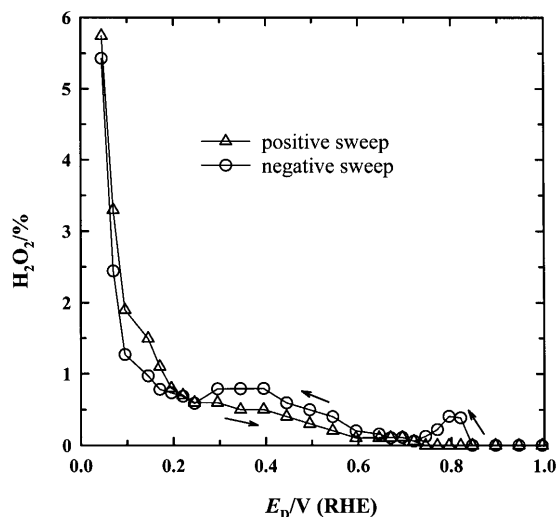

Fig. 5. Fraction of H_2O_2 formation during O_2 reduction on Pt/Vulcan (14 μg_{Pt} cm^{-2}) at 60°C in 0.5 M H_2SO_4 saturated with 1 bar O_2. Calculated from the data in Fig. 4 (at 1600 rpm) using Eq. (11) with $N = 0.19$ (triangles, positive sweep; circles, negative sweep).
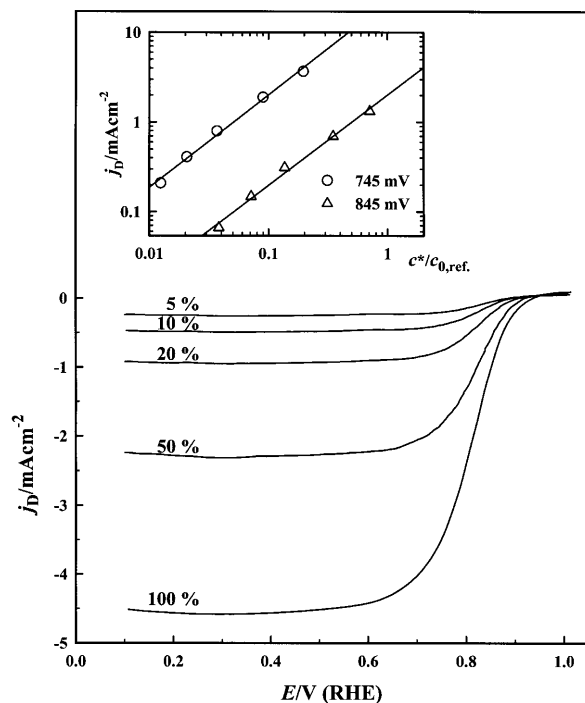
Fig. 6. Potentiodynamic (5 mV s^{-1}) oxygen reduction current densities (positive sweeps) at different O$_2$ partial pressures at 60°C and 1600 rpm on a thin-film Pt/Vulcan R(R)DE (14 μg$_{Pt}$ cm^{-2}). Inset: double-logarithmic plot of disk current density versus oxygen surface concentration (c^* referenced to c_0 for 1 bar O$_2$) for two different potentials (circles, 745 mV; triangles, 845 mV).
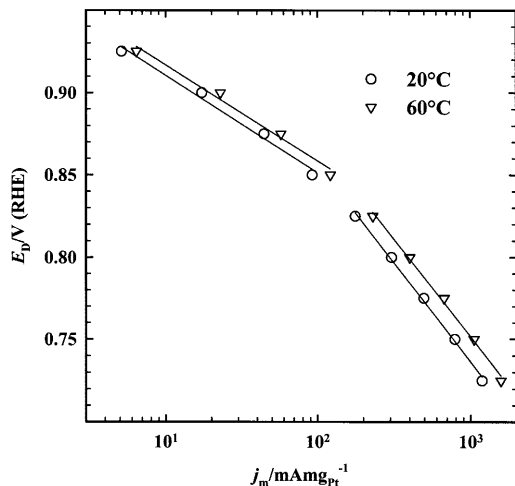

Fig. 7. Mass transport corrected mass-specific current densities for the orr on a Pt/Vulcan thin-film R(R)DE (14 μg$_{Pt}$ cm^{-2}), obtained from positive sweeps (5 mV s^{-1}, 1600 rpm) in 0.5 M H$_2$SO$_4$ saturated with O$_2$ at 20°C (circles) and 60°C (triangles).

solution phase O$_2$ can be determined from measurements with different O$_2$ partial pressures.

Fig. 6 shows the potentiostatic (5 mV s^{-1}) oxygen reduction current densities at the thin-film Pt/Vulcan R(R)DE measurements for different O$_2$ concentrations (60°C, 1600 rpm). The positive shift of the oxygen

reduction current is equivalent qualitatively to a positive reaction order for the orr with respect to O$_2$ partial pressure. Under the condition that Henry's law is valid, the O$_2$ concentration near the electrode surface, c^*, can be determined experimentally from the measured disk current density, j_D, by Eq. (12) [15]:

$$c^* = c_0\left(1 - \frac{j_D}{j_d}\right) \tag{12}$$

Assuming a simple power-law relation for the orr with a potential dependent rate constant, k_E, the reaction order, n, can be determined from a double-logarithmic plot of j_D versus c^* following Eq. (13):

$$j_D = k_E(c^*)^n \tag{13}$$

This is shown in the inset of Fig. 6 for two different electrode potentials, where c^* is normalized to the O$_2$ saturation concentration in the electrolyte for pure O$_2$ at 1 bar, c_0. In the potential range in which O$_2$-reduction is under mixed kinetic-diffusion control (ca. 745 to 845 mV), the reaction order determined from this analysis is practically unity (1.00 $\pm$ 0.05). This result is in accordance with the reaction order determined on polycrystalline Pt in acid and neutral solutions [1,26,30] as well as for carbon supported platinum catalyst in a PEMFC [31,32], supporting a similar reaction mechanism in all of these cases.

4.4. Kinetic analysis of the orr on Pt/Vulcan

Having confirmed that the orr on the Pt/Vulcan catalyst obeys first order kinetics, the kinetic current densities can be evaluated from the thin-film R(R)DE measurements applying Eq. (2). As has been mentioned in Section 3.1, Nafion® film resistances can be neglected up to ca. 1.5 A mg$_{Pt}^{-1}$. Fig. 7 shows the Tafel plots for the mass transport corrected mass-specific current densities at 20°C and 60°C for O$_2$ reduction on the Pt/Vulcan catalyst, obtained from the positive-going sweep direction at 1600 rpm. Even though it is clear that the Tafel slope for the orr is changing continuously in the potential range examined [23,33], we fitted the experimental data to the two Tafel slope regions at low and high overpotentials in order to facilitate the comparison

Table 1
Low- and high-current density Tafel slopes (TS) for the orr on Pt/Vulcan (14 μg$_{Pt}$ cm^{-2}; two independent experiments) as a function of temperature in 0.5 M H$_2$SO$_4$, saturated with pure O$_2$ at 1 bar

T/°C	TS/mV dec^{-1} for $E >$ 0.85 V	TS/mV dec^{-1} for $E < 0.85$ V
20	$-63 \pm 5\%$	$-120 \pm 1\%$
30	$-62 \pm 2\%$	$-123 \pm 1\%$
40	$-60 \pm 3\%$	$-122 \pm 1\%$
60	$-58 \pm 1\%$	$-115 \pm 3\%$

Table 2
Comparison of the O_2 reduction activity of Pt/Vulcan determined by the thin-film RDE technique with literature data reported for carbon-supported Pt, polycrystalline bulk Pt, and Pt single crystals at elevated temperature; current densities are referred to the electrochemically active Pt surface area (μA $(cm^{-2})_{real}$) at 1 bar O_2 and at a constant electrode potential of 0.90 and 0.85 V (vs. RHE), respectively

Method	Electrode	Electrolyte	$T/^\circ C$	j at 0.90 V	j at 0.85 V	Reference
Thin-film RDE	20% Pt/Vulcan	0.5 M H_2SO_4	60	35	190	this work
GDE [a]	10% Pt/carbon [b]	1.5 M H_2SO_4	60		80	[43]
GDE [a]	5% Pt/carbon [b]	1.0 M H_2SO_4	50	20		[37]
PEM	20% Pt/Vulcan	Dow membrane	60	90		[31]
PEM	20% Pt/Vulcan	Nafion® 115	60	330		[42]
RDE	polycrystalline Pt	0.5 M H_2SO_4	60	110	400	this work
RDE	faceted Pt-disks [c]	1.0 M H_2SO_4	62	6–8	16	[34]
RDE	Pt(111)	0.05 M H_2SO_4	60	80	650	[24]
RDE	Pt(100)	0.05 M H_2SO_4	60	480	1450	[24]
RDE	Pt(110)	0.05 M H_2SO_4	60	1900	5400	[24]
Thin-film RDE	20% Pt/Vulcan	0.5 M $HClO_4$	60	65	510	this work

[a] Teflon-bonded gas diffusion electrodes.
[b] Unspecified carbon substrate.
[c] Bulk Pt rotating disk electrodes, faceted to yield (111) and (100)-type surfaces.

with literature data (e.g. Refs. [34,35]). The resulting Tafel slopes at different temperatures between 20°C and 60°C are summarized in Table 1. They are in good conformity with Tafel slopes for single crystal Pt electrodes [24], polycrystalline Pt [36], carbon supported Pt catalysts [37], and the platinum | Nafion® interface [35,38], with values around $-2.3RT/F$ at low overpotentials ($E > 0.85$ V) and values of ca. $-2 \times 2.3RT/F$ at high overpotentials ($E < 0.80$ V). There were no significant differences in the Tafel slopes between the positive and the negative sweep directions, in contrast to findings in a recent Pt microelectrode | Nafion® interface study [33]. Most likely these differences in the latter study result from a contamination effect from the polymer electrode.

In order to compare the activity of different electrocatalysts in PEM fuel cells or gas diffusion electrodes, it is common to take the kinetically controlled current density at a potential of 0.9 V, where influences of mass transport are negligible (due to H_2 cross-over this is not valid for the relatively thin Gore Select membranes). At 0.9 V and 60°C, the mass-specific current density in our experiments is 23 mA mg_{Pt}^{-1} (Fig. 7), which agrees with 25 mA mg_{Pt}^{-1} obtained for supported Pt catalysts with similar particle size in a PEM fuel cell at 60°C [31] and 50°C [4] (all at 1 bar O_2), respectively. Similar mass-specific current densities were also observed in gas diffusion electrodes in sulfuric acid electrolyte (ca. 20 mA mg_{Pt}^{-1} in 1 M H_2SO_4 at 50°C [37]; ca. 16 mA mg_{Pt}^{-1} in 3 M H_2SO_4 at 60°C [39]). Overall, the thin-film R(R)DE data on Pt/Vulcan are consistent with typically reported fuel cell data.

For a more detailed comparison of the orr activity of the Pt/Vulcan catalyst with polycrystalline and single-crystal Pt electrodes and, particularly, with fuel cell data, the catalyst utilization has to be considered.

Hence, the orr activity must be normalized to the electrochemically active surface area (i.e. the *real* surface area in μA $(cm^{-2})_{real}$) using experimentally determined roughness factors. This is shown in Table 2 for two different cathode potentials (0.90 and 0.85 V) at temperatures around 60°C. Quite clearly, the thin-film Pt/Vulcan R(R)DE data (first line, Table 2) are in good agreement with data from gas diffusion electrodes in sulfuric acid electrolyte (lines 2 and 3, Table 2), but are significantly lower than the current densities extracted from PEM fuel cells (lines 4 and 5, Table 2). The latter fact might be due to either anion adsorption effects [23] which are absent in the case of the polymer electrolyte and/or to a higher oxygen concentration in the Nafion® ionomer [27] which would be expected to enhance the orr activity compared to the activity in aqueous acidic electrolytes.

Based on Pt single-crystal data [23], a reduced orr activity due to anion adsorption should be most pronounced on Pt(111) and Pt(100) sites so that the higher orr activity on the polycrystalline Pt electrode (line 6 in Table 2) compared to both the Pt/Vulcan catalyst and the faceted Pt(111) and Pt(100) electrodes in 1.0 M H_2SO_4 (line 7 in Table 2) is consistent with anion adsorption effects from the sulfuric acid electrolyte. In the more dilute 0.05 M H_2SO_4, much higher orr activities are reported for all the low-index Pt surfaces (lines 8–10, Table 2), in the order Pt(111) < Pt(100) < Pt(110). Since the activity of all low-index Pt single-crystal surfaces is maximized in a non-specifically adsorbing $HClO_4$ electrolyte [23], significantly higher orr activity should be expected for the Pt/Vulcan catalyst in 0.5 M $HClO_4$ compared to 0.5 M H_2SO_4. As is evident from Fig. 8, the mass-specific current densities in the non-specifically adsorbing electrolyte are indeed significantly higher than in 0.5 M H_2SO_4 (last versus first line in Table 2), while the fraction of H_2O_2 forma-

tion is essentially the same. In the 0.5 M HClO₄ electrolyte, the current densities referenced to the real surface area observed for the Pt/Vulcan catalyst are now in good agreement with the data recorded for a Pt(111) single crystal at the same temperature in dilute sulfuric electrolyte (see Table 2). This is consistent with the cubo-octahedral model for supported Pt nanoparticles, which would predict a predominant fraction of (111) faces on the Pt/Vulcan catalyst [12]. The still lower activity of the Pt/Vulcan catalyst in 0.5 M HClO₄ in our experiments compared to the PEM-FC data

Fig. 8. Mass transport corrected mass-specific current densities for the orr on a Pt/Vulcan thin-film R(R)DE (14 μg_{Pt} cm^{-2}), obtained from positive sweeps (5 mV s^{-1}, 1600 rpm) in 0.5 M H₂SO₄ (circles) and in 0.5 M HClO₄ (triangles) saturated with O₂ at 60°C.

Fig. 9. Arrhenius plots for the mass-specific current densities for the orr at an overpotential of 350 mV for the oxygen reduction on a Pt/Vulcan thin-film R(R)DE (14 μg_{Pt} cm^{-2}), obtained from positive sweeps (5 mV s^{-1}, 1600 rpm) in 0.5 M H₂SO₄ (circles) and 0.5 M HClO₄ (triangles), respectively.

listed in Table 2 might then be due to the higher O₂ solubility in (recast) Nafion® versus the aqueous electrolyte [1].

In the last part of this kinetic analysis we will determine the activation energies for the orr on the Pt/Vulcan catalyst in 0.5 M H₂SO₄ and 0.5 M HClO₄, respectively. The activation enthalpies (ΔH^*) are evaluated at fixed overpotentials using the Arrhenius equation (Eq. (14)) [15].

$$\left. \frac{\partial(\log j_k)}{\partial(1/T)} \right|_\eta = \frac{\Delta H^*}{2.3R} \tag{14}$$

The overpotential with respect to the O₂/H₂O equilibrium potential at each temperature, $\eta_{O_2(T)}$, is determined from the potential measured on the reversible hydrogen electrode scale at the respective temperature, $E_{RHE(T)}$, and the reversible H₂/O₂ cell potential, $E_{cell(T)}$:

$$\eta_{O_2(T)} = E_{cell(T)} - E_{RHE(T)} = \frac{-\Delta G_{H_2/O_2(T)}}{2F} - E_{RHE(T)} \tag{15}$$

where the temperature dependence of $\Delta G_{H_2/O_2(T)}$ is given by [35]

$$\Delta G_{H_2/O_2(T)} = -295600 - 33.5 \ln(T) + 388.4T$$
$$\text{in J mol}^{-1} \tag{16}$$

When working in an open system, the deviations of the reversible H₂/O₂ cell potential due to a decrease in oxygen partial pressure with increasing temperature are negligible in the temperature range between 20°C and 60°C.

The Arrhenius plots for $\eta = 350$ mV are shown in Fig. 9 for Pt/Vulcan in both 0.5 M H₂SO₄ and 0.5 M HClO₄. The activation enthalpies determined from least squares regressions are ≈ 26 kJ mol^{-1} in 0.5 M H₂SO₄ and ≈ 28 kJ mol^{-1} in 0.5 M HClO₄. Essentially identical values were determined at $\eta_{O_2(T)} = 400$ mV (data not shown), which is still within the region of low Tafel slopes (see Fig. 7). This indicates that the rate-determining step (rds) in the orr mechanism is identical in both electrolytes. Closely following Grgur et al. [24], who found a similar value of ca. 20 kJ mol^{-1} on all three low index Pt single crystal surfaces (0.05 H₂SO₄, 0.8 V), this value reflects the first electron transfer as the rds.

The activation enthalpies from our study are in good agreement with the values reported for polycrystalline platinum in sulfuric acid at pH 1 and 0.8 V [36] and in perchloric acid at 0.8 V (pH 1.9) [40], ~ 25 kJ mol^{-1} and ~ 20 kJ mol^{-1}, respectively. The same activation enthalpy of ≈ 28 kJ mol^{-1} was also found in a microelectrode study for the orr at the Pt│Nafion® interface in the region of low Tafel slopes [35]. A significantly larger activation enthalpy of ≈ 60 kJ mol^{-1} was determined by Mukerjee et al. [32] at 0.9 V
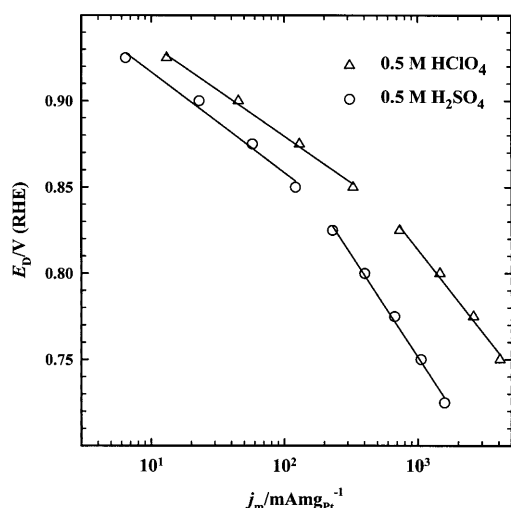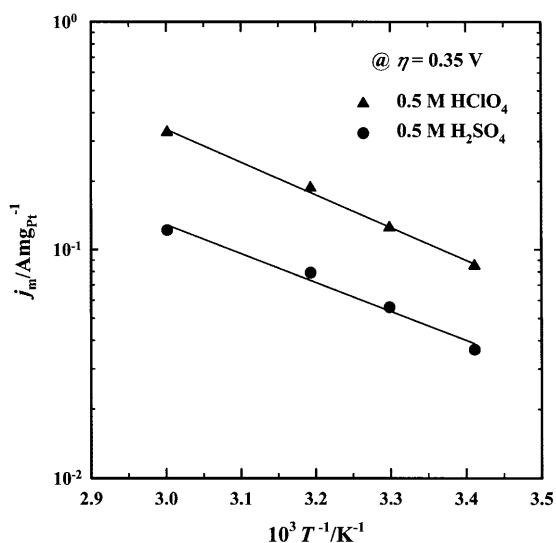
in a PEM-FC. One can only speculate on the reason for this deviation, but it might be related to water management effects in the cathode catalyst layer (i.e. flooding). Similar activation enthalpies of ≈ 58 kJ mol^{-1} were also observed by Beattie et al. [38] studying the Pt | Nafion® 117 interface by using the microelectrode technique. The authors explain their higher activation enthalpies compared to Parthasarathy et al. [35] with organic impurities at the Pt | polymer interface.

4.5. Comparison with PEM-FC data

In the last section we try to compare our pure kinetic data for the oxygen reduction reaction with performance data of real fuel cells. Since the overpotential for H$_2$ oxidation is negligible in the case of pure H$_2$ feed [1], the performance of H$_2$/air fuel cells is always limited by both the kinetics of the orr and effects related to mass transport of water (i.e. flooding and drying out of the membrane/catalyst layer) and O$_2$. These mass transport resistances become reduced as the thickness of the membrane and the cathode catalyst layer is decreased, as was shown in a study by Wilson et al. [41] using Nafion® 112 and ultra-low cathode loadings of 0.15 mg$_{Pt}$ cm^{-2}. Under these conditions fuel cell performance data and the kinetic current densities determined via thin-film RDE measurements should become comparable. At a cell temperature of 80°C and an air pressure of 5 bar (i.e. an O$_2$-pressure of ca. 1 bar), their performance data indicate that mass transport resistances are negligible for current densities ≤ 0.5 A cm^{-2}. At 0.5 A cm^{-2} the cell potential, without ohmic losses (*IR*-free), amounted to 800 mV. Assuming an anode overpotential of ca. 10 mV, the oxygen reduction activity corresponds to 3.3 A mg$_{Pt}^{-1}$ at a cathode potential of ca. 810 mV (on the RHE scale). For comparison, the mass specific current density at 810 mV on the same Pt/Vulcan catalyst in 0.5 M HClO$_4$ at 60°C is only 1.1 A mg$_{Pt}^{-1}$ (see Fig. 8), a difference which is too large to be accounted for by the difference in temperature (note that the activation energy of ≈ 28 kJ mol^{-1} was determined at constant $\eta_{O_2(T)}$ and that $E_{cell(T)}$ decreases by 17 mV going from 60° to 80°C [35] so that the increase in activity at constant cell voltage is less than at constant $\eta_{O_2(T)}$). A likely reason for the seemingly higher activity in this PEM-FC measurement is the roughly three-fold higher oxygen solubility in the recast Nafion® ionomer in contact with the cathode catalyst [1], in combination with the first order oxygen reduction kinetics (see Section 3.3). This would also be consistent with the higher oxygen reduction activity reported by Lee et al. [42] (5th line in Table 2) in a PEM-FC at 60°C compared to the R(R)DE data in 0.5 M HClO$_4$ (last line in Table 2).

Assuming that the oxygen reduction activity in a PEM-FC (with recast Nafion® ionomer in the cathode catalyst layer) is indeed enhanced by a factor of three

compared to the 0.5 M HClO$_4$ electrolyte, one can estimate the ideal H$_2$/air PEM performance (100% utilization, no ohmic and mass transport resistances) from the data in Fig. 8. Assuming a Pt loading of 0.2 mg$_{Pt}$ cm^{-2} (20 wt.% Pt/Vulcan) and a current density of 1 A cm^{-2}, the required mass-specific activity for a PEM-FC is 5 A mg$_{Pt}^{-1}$. If the cell is operated at 60°C with humidified air at 3 bar total cathode pressure (with a water partial pressure at 60°C of 0.8 bar, this leads to an average O$_2$ partial pressure of 0.45 bar), the oxygen reduction activity on a 20% Pt/Vulcan catalyst would be $0.45 \times 3 = 1.35$ times larger than what is shown in Fig. 8 for the 0.5 M HClO$_4$ electrolyte (reduced O$_2$ partial pressure but higher solubility in the recast Nafion® ionomer). Therefore, the predicted ideal cathode potential under these fuel cell operating conditions would be ca. 750 mV (from Fig. 8 at a mass-specific current density of $5/1.35 = 3.7$ A mg$_{Pt}^{-1}$). This should be considered as the kinetic limit in the absence of ohmic and mass transport resistances at 100% catalyst utilization.

5. Conclusion

We proved that the thin-film RRDE method for supported catalysts can be applied successfully for characterizing the electrocatalytic activity and kinetic behavior of supported high surface area catalysts in the orr. The diffusion resistance of the thin Nafion® film to fix the catalyst particles to the carbon substrate is negligible, i.e. the kinetic current densities can be determined directly from the measured currents without extensive mathematical modeling.

The potential- and rotation-rate independent, well defined collection efficiency for the thin film RRDE configuration enables one to quantify the amount of hydrogen peroxide produced during oxygen reduction, i.e. to quantify the ratio between the four-electron versus two-electron reaction pathway, an important issue for screening of new catalysts.

The obtained mass-specific current densities at 0.9 V and 0.85 V in 0.5 M H$_2$SO$_4$ are in good agreement with literature data from gas diffusion electrodes in sulfuric acid. The higher activities in PEM fuel cells and a clearly higher activity measured in this work on a thin film RDE in 0.5 M HClO$_4$ point to a significant anion adsorption effect in 0.5 M H$_2$SO$_4$ as well as to possible enhancing effects of the higher oxygen solubility in Nafion® electrolytes. The activation enthalpies and reaction orders obtained are in good agreement with values reported in the literature.

References

[1] S. Gottesfeld, T.A. Zawodzinski, in: R.C. Alkire, H. Gerischer, D.M. Kolb, C.W. Tobias (Eds.), Advances in Electrochemical Science and Engineering, vol. 5, Wiley-VCH, Weinheim, 1997, Chapter 4.

[2] T.J. Schmidt, U.A. Paulus, H.A. Gasteiger, N. Alonso-Vante, R.J. Behm, J. Electrochem. Soc. 147 (2000) 2620.

[3] F. Gloaguen, F. Andolfatto, R. Durand, P. Ozil, J. Appl. Electrochem. 24 (1994) 863.

[4] F. Gloaguen, P. Convert, S. Gamburzev, O.A. Velev, S. Srinivasan, Electrochim. Acta 43 (1998) 3767.

[5] S.Lj. Gojkovic, S.K. Zecevic, R.F. Savinell, J. Electrochem. Soc. 145 (1998) 3713.

[6] T.J. Schmidt, H.A. Gasteiger, G.D. Stäb, P.M. Urban, D.M. Kolb, R.J. Behm, J. Electrochem. Soc. 145 (1998) 2354.

[7] T.J. Schmidt, H.A. Gasteiger, R.J. Behm, J. Electrochem. Soc. 146 (1999) 1296.

[8] E. Claude, T. Addou, J.-M. Latour, P. Aldebert, J. Appl. Electrochem. 28 (1998) 57.

[9] U.A. Paulus, Diploma Thesis, University of Ulm, Germany, 1998.

[10] M. Peuckert, T. Yoneda, B. Dalla, M. Boudart, J. Electrochem. Soc. 13 (1986) 944.

[11] P. Lööf, B. Stenbom, H. Nordén, B. Kasemo, J. Catal. 144 (1993) 60.

[12] K. Kinoshita, Electrochemical Oxygen Technology, Wiley, New York, 1992.

[13] D.R. Lawson, L.D. Whiteley, C.R. Martin, M.N. Szentimay, J.I. Song, J. Electrochem. Soc. 135 (1988) 2247.

[14] M. Watanabe, H. Igarashi, K. Yosioka, Electrochim. Acta 40 (1995) 329.

[15] A.J. Bard, L.R. Faulkner, Electrochemical Methods — Fundamentals and Applications, Wiley, New York, 1980.

[16] J.R. Welty, C.E. Wicks, R.E. Wilson, Fundamentals of Momentum, Heat and Mass Transfer, 3rd edn, Wiley, New York, 1984.

[17] D.R. Lide, CRC Handbook of Chemistry and Physics, 76th edn, CRC Press, Boca Raton, FL, 1995.

[18] W.J. Albery, M.L. Hitchman, Ring-Disc Electrodes, Clarendon Press, Oxford, 1971.

[19] N.A. Anastasijevic, V.B. Vesovic, R.R. Adzic, J. Electroanal. Chem. 229 (1987) 305.

[20] E. Yeager, Electrochim. Acta 29 (1984) 1527.

[21] E. Yeager, J. Mol. Catal. 38 (1986) 5.

[22] N.M. Markovic, H.A. Gasteiger, P.N. Ross, J. Phys. Chem. 99 (1995) 3411.

[23] N.M. Markovic, H.A. Gasteiger, P.N. Ross, J. Electrochem. Soc. 144 (1997) 1591.

[24] B.N. Grgur, N.M. Markovic, P.N. Ross, Jr., Can. J. Chem. 75 (1997) 1465.

[25] N. Giordano, E. Passalacqua, A.S. Aricò, L. Pino, V. Antonucci, M. Vivaldi, K. Kinoshita, Electrochim. Acta 36 (1991) 1979.

[26] A. Damjanovic, M.A. Genshaw, J.O.M. Bockris, J. Electrochem. Soc. 114 (1967) 466.

[27] S. Gottesfeld, I.D. Raistrick, S. Srinivasan, J. Electrochem. Soc. 134 (1987) 1455.

[28] N.M. Markovic, H.A. Gasteiger, B.N. Grgur, P.N. Ross, J. Electroanal. Chem. 467 (1999) 157.

[29] N.M. Markovic, H.A. Gasteiger, P.N. Ross, J. Phys. Chem. 100 (1996) 6715.

[30] K.J. Vetter, Electrochemical Kinetics, Academic Press, New York, 1967.

[31] S. Mukerjee, S. Srinivasan, J. Electroanal. Chem. 357 (1993) 201.

[32] S. Mukerjee, S. Srinivasan, M.P. Soriaga, J. Phys. Chem. 99 (1995) 4577.

[33] F.A. Uribe, T.E. Springer, S. Gottesfeld, J. Electrochem. Soc. 139 (1992) 765.

[34] C.F. Zinola, L. Castro, A.J. Arvia, Electrochim. Acta 39 (1994) 1951.

[35] A. Parthasarathy, S. Srinivasan, A.J. Appleby, C.R. Martin, J. Electrochem. Soc. 139 (1992) 2530.

[36] A. Damjanovic, D.B. Sepa, Electrochim. Acta 35 (1990) 1157.

[37] J. Bett, J. Lundquist, Electrochim. Acta 18 (1973) 343.

[38] P.S. Beattie, V.I. Basura, S. Holdcroft, J. Electroanal. Chem. 468 (1999) 180.

[39] M. Watanabe, K. Makita, U. Hiroyuki, S. Motoo, J. Electroanal. Chem. 197 (1986) 195.

[40] D.B. Sepa, M.V. Vojnovic, L. Vracar, A. Damjanovic, Electrochim. Acta 31 (1986) 91.

[41] M.S. Wilson, J. Valerio, S. Gottesfeld, Electrochim. Acta 40 (1995) 355.

[42] S.J. Lee, S. Mukerjee, J. McBreen, Y.W. Rho, Y.T. Kho, T.H. Lee, Electrochim. Acta 43 (1998) 3693.

[43] M. Watanabe, S. Saegusa, P. Stonehart, Chem. Lett. (1988) 1487.